Molybdenum nitride for the direct decomposition of NO

H. He [a,b], H.X. Dai [a], K.Y. Ngan [a] and C.T. Au [a,*]

[a] *Department of Chemistry, Hong Kong Baptist University, Kowloon Tong, Hong Kong*
E-mail: pctau@hkbu.edu.hk
[b] *College of Environmental and Energy Engineering, Beijing Polytechnic University, Beijing, 100022, PR China*

Received 24 August 2000; accepted 28 November 2000

The physico-chemical properties of passivated γ-Mo_2N have been investigated. The material showed high activities for NO direct decomposition: nearly 100% NO conversion and 95% N_2 selectivity were achieved at 450 °C. The amount of O_2 taken up by γ-Mo_2N increased with temperature rise and reached 3133.9 μmol g^{-1} at 450 °C; we conclude that formation of $Mo_2O_xN_y$ occurred. This oxygen-saturated γ-Mo_2N material was catalytically active: NO conversion and N_2 selectivity were 89 and 92% at 450 °C. We found that by means of H_2 reduction at 450 °C, $Mo_2O_xN_y$ could be reduced back to γ-Mo_2N and the oxidation/reduction cycle is repeatable; such a behaviour and the high oxygen capacity (3133.9 μmol g^{-1}) of γ-Mo_2N suggest that γ-Mo_2N is a promising catalytic material for automobile exhaust purification.

KEY WORDS: γ-Mo_2N catalyst; $Mo_2O_xN_y$; NO decomposition; oxygen storage; isotope ^{15}NO pulse

1. Introduction

Nitrogen oxides (NO_x) are known pollutants of the atmosphere [1,2]. The control of NO_x emission has been a great challenge in environment protection. Catalytically, NO_x can be eliminated either by the direct decomposition or by the selective reduction of NO_x using ammonia, hydrocarbons, carbon monoxide, and/or hydrogen as reductants. Although the selective catalytic reduction of NO_x with ammonia is effective, the process is only suitable for the removal of NO_x from a stationary source; furthermore, the use of ammonia is expensive and will inevitably cause secondary pollution. The direct catalytic decomposition of NO_x is a promising route because no other additives are needed and the major products, O_2 and N_2 (a little amount of N_2O is also formed) are benign to the environment.

Due to its high surface area and unique catalytic properties (those similar to group VIII metals) in many hydrogen-involving reactions [3], molybdenum nitride has attracted much attention in heterogeneous catalysis. For example, the material shows good catalytic activities in carbon monoxide hydrogenation [4], ammonia synthesis [5], and ethane hydrogenolysis [4] as well as in hydrodesulfurization and hydrodenitrogenation (HDN) reactions [6–10]. It has been reported that the adsorptions of O_2 (at ca. 25 °C) and H_2 (at ca. 230 °C) on γ-Mo_2N were dissociative [11]. Li et al. [12] detected a large amount of N_2 when γ-Mo_2N was exposed to NO or NH_3. Based on these characteristics of γ-Mo_2N, we envisage that the material could be a good catalyst for the direct decomposition of NO.

In this paper, we present the catalytic performance of γ-Mo_2N for NO direct decomposition in pulse reactions. The O_2- and NO-uptake behaviors of this catalyst at different temperatures are also reported. The techniques used in the investigation were XRD (X-ray diffraction), TPD (temperature-programmed desorption), and TPR (temperature-programmed reduction) as well as ^{15}NO pulse reaction. A reaction mechanism for NO decomposition over γ-Mo_2N has been proposed.

* To whom correspondence should be addressed.

2. Experimental

The γ-Mo_2N sample was synthesized by adopting the TPN (temperature-programmed nitridation) method [11]. The starting material MoO_3 (99.5%, Aldrich) was pressed into pellets, crushed, and sieved to the size of 40–60 mesh. Then 2.0 g of the particles was placed in a microreactor (i.d. = 4 mm) and a flow of NH_3 (70 ml min^{-1}, Solkatronic) was introduced into the system. Initially the sample was linearly heated from room temperature to 350 °C over a period of approximately 30 min. Subsequently, the temperature was raised from 350 to 450 °C and from 450 to 650 °C at a rate of 0.6 and 1.6 °C min^{-1}, respectively, and from 650 to 700 °C at a temperature ramp of 1.6 °C min^{-1}. After being kept at 700 °C for 1 h, the material was rapidly cooled to room temperature in NH_3. The γ-Mo_2N was then purged in He (20 ml min^{-1}) for 10 min and passivated (at 20 °C) in a mixture of 1% O_2–99% He overnight. A H_2-treated sample was prepared by heating the passivated material in H_2 at 450 °C for 1 h.

The NO decomposition reaction and the isotope experiments were carried out in a quartz tube microreactor (i.d. = 4 mm) by pulsing NO (99%) and ^{15}NO (99%), respectively, into the reactor with He (15 ml min^{-1}, 99.999%) being the carrier gas. The catalyst (50 mg) was packed in the middle of the reactor between two quartz wool plugs. The reaction temperature was monitored by a thermocouple located

at the bed of the catalyst and regulated from 50 to 450 °C at an interval of 50 °C. The size of each pulse was 50.0 μl. Before pulsing ^{14}NO and ^{15}NO, the passivated γ-Mo_2N catalyst was heated in a flow of He (20 ml min^{-1}) at 450 °C for 1 h in order to scour away the surface NH_x adspecies accumulated during catalyst preparation. The blank runs with only quartz wool plugs in the reactor indicated that NO decomposition was negligible below 450 °C. A Porapak Q column was employed to separate N_2 from NO. Isotopic species such as $^{15}N_2$ ($m/z = 30$) and $^{14}N^{16}O$ ($m/z = 30$) were then quantitatively analyzed by an on-line mass spectrometer (HP G-1800A). The data obtained at the 10th pulse were used for activity calculation; that was when the reaction had become stabilized.

The TPR and TPD experiments were carried out in a similar microreactor. Before performing the H_2-TPR investigation, a γ-Mo_2N sample (50 mg) was heated to 150 °C in N_2 and maintained at this temperature for 1 h. Before performing a NO-TPD experiment, the sample was first pre-treated *in situ* in NO (20 ml min^{-1}) at 450 °C for 1 h, followed by cooling to room temperature in the same atmosphere and purging with He for 10 min. After being cooled to room temperature, the sample was heated from 30 to 900 °C at a rate of 10 °C min^{-1}. The flow rates of the 5% H_2–95% N_2 (v/v) mixture (for TPR) and He (for TPD) were 50 and 20 ml min^{-1}, respectively. For TPD studies, the effluent gases were monitored on-line by a mass spectrometer, whereas for TPR investigations, they were analyzed by a thermal conductivity detector.

The O_2 and NO uptake experiments were performed in the same quartz microreactor. The sample (50 mg) was first treated in He (20 ml min^{-1}) at 450 °C for 1 h, and then cooled in He to room temperature. We kept pulsing O_2 or NO onto the sample until no observable change in O_2 or NO signal intensity was detected.

The specific surface areas and the pore size distribution of the γ-Mo_2N material were measured, respectively, by the BET and desorption methods using a Nova 1200 instrument. The sample was first treated in vacuum (1.1×10^{-3} Torr) at 350 °C for 2 h before BET and pore size distribution measurements. The XRD experiments were carried out on an X-ray diffractometer (Rigaku D-Max Rotaflex) with Cu Kα radiation and Ni filter.

3. Results

3.1. Physico-chemical properties

3.1.1. Pore size and specific surface area

The pore size distribution of passivated γ-Mo_2N is shown in figure 1. Obviously, the particles exhibited a rather narrow distribution (16–70 Å) in pore size; the pore volume reached a maximum value of 5.44 ml g^{-1} at a pore size of 38.5 Å. Above 70 Å, the pore volume became very small. The average pore diameter and the specific surface area of the material were 43.1 Å and 108 m^2 g^{-1}, respectively. According

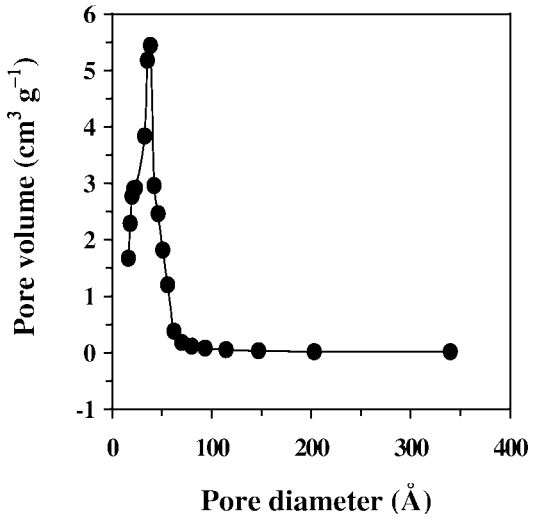

Figure 1. Pore size distribution of passivated γ-Mo_2N.

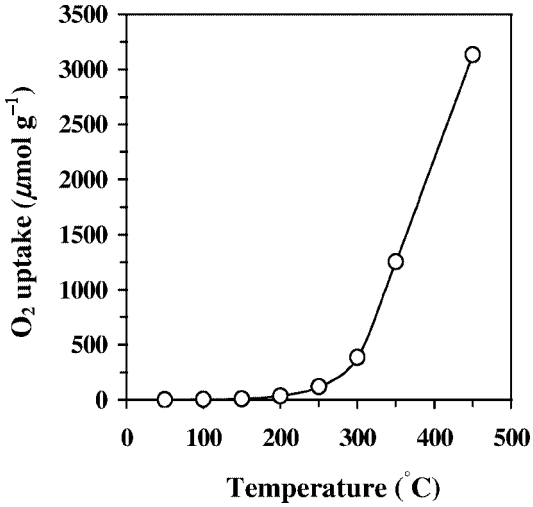

Figure 2. Accumulative O_2 uptake over passivated γ-Mo_2N.

to equation (1), the average particle size, D_p, of passivated γ-Mo_2N was estimated to be 5.91 nm:

$$D_p = f_p/S_g\rho, \tag{1}$$

where f_p (a characteristic of particle shape) is 6 for spherical and cubic particles, S_g is the surface area, and ρ (density of material) is 9.4 g cm^{-3} for γ-Mo_2N [13].

3.1.2. Oxygen and nitric oxide uptakes

Figures 2 and 3 show the amounts of O_2 and NO uptakes over γ-Mo_2N versus temperature, respectively. From figure 2, one can observe that at 150 and 200 °C, the accumulative amounts of O_2 absorbed by the material were 8.0 and 37.4 μmol g^{-1}, respectively; at or above 300 °C, the O_2 uptake increased abruptly: it was 382.9 μmol g^{-1} at 300 °C and 3133.9 μmol g^{-1} at 450 °C. In order to investigate the oxygen storage capacity of γ-Mo_2N, a sample treated with O_2 at 450 °C was reduced in H_2 (15 ml min^{-1}) at 450 °C for 20 min and purged with He (15 ml min^{-1}) for 30 min (to remove the adsorbed hydrogen), and then O_2 was

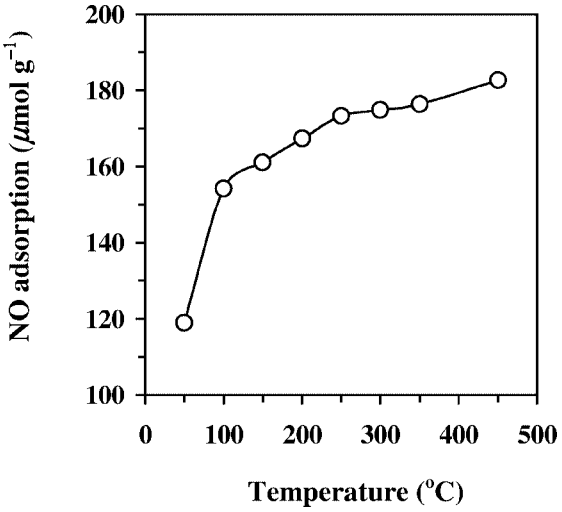

Figure 3. Accumulative NO uptake over passivated γ-Mo_2N.

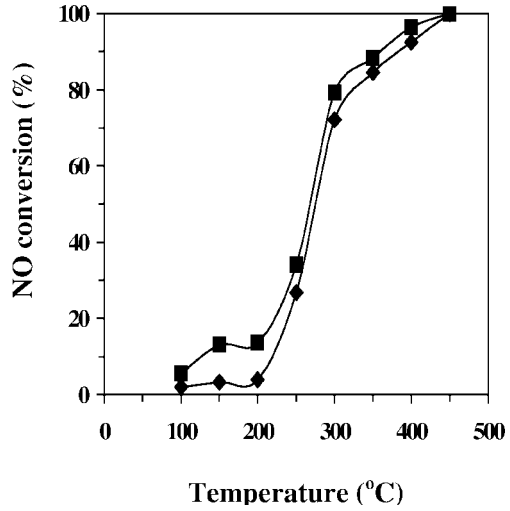

Figure 4. NO conversions over passivated (♦) and H_2-treated (■) γ-Mo_2N.

pulsed onto the sample until the sample was saturated with oxygen. Since the adsorbed hydrogen had been removed completely as reflected by the absence of H_2O in the effluent during O_2 pulsing, the oxygen consumed should reflect the exact amount of oxygen uptake of the sample. The amount of oxygen removed in H_2 reduction at 450 °C was ca. 2914.5 μmol g^{-1}, ca. 93% of the original oxygen uptake (i.e., 3133.9 μmol g^{-1}) of the sample. We repeated the H_2 reduction and O_2-pulsing cycle three times and obtained similar results. On the other hand, the accumulative amounts of NO adsorption over γ-Mo_2N were estimated to be 119.0 and 182.7 μmol g^{-1}, respectively, at 50 and 400 °C (figure 3).

3.2. Activities for NO decomposition

3.2.1. Over passivated and H_2-treated γ-Mo_2N

Figure 4 shows the performance of the passivated and H_2-treated γ-Mo_2N samples in NO pulsing as related to reaction temperature. It was observed that the performance

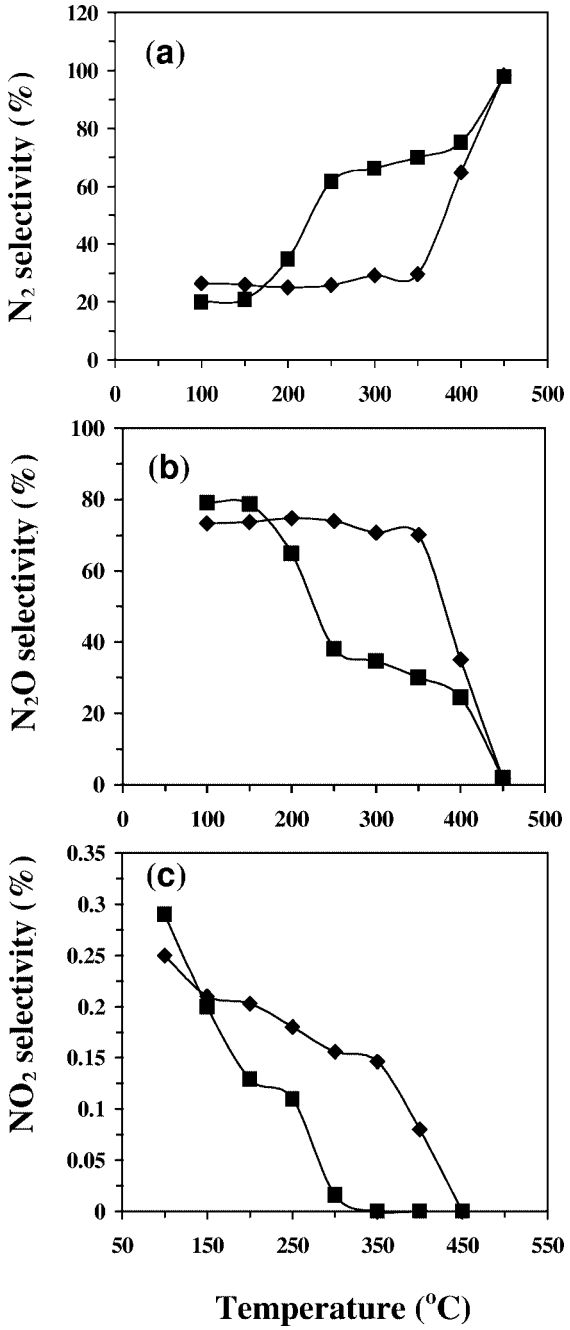

Figure 5. (a) N_2, (b) N_2O, and (c) NO_2 selectivities in NO decomposition over passivated (♦) and H_2-treated (■) γ-Mo_2N.

of the latter was slightly better than that of the former. At 200 °C, NO conversion was 13.6% over the latter and 3.9% over the former; at 300 °C, NO conversion was 79.3% over H_2-treated γ-Mo_2N, whereas over passivated γ-Mo_2N, it was 72.2%. At or above 450 °C, nearly 100% NO conversion was observed over the two materials. Figure 5 (a)–(c) shows the selectivities of N_2, N_2O, and NO_2 versus temperature, respectively. Compared to a H_2-treated γ-Mo_2N sample, a passivated one is less capable of producing N_2 within the temperature range of 250–350 °C: N_2 selectivities being ca. 26% over passivated γ-Mo_2N and ca. 65% over H_2-treated γ-Mo_2N. Below 200 or above 400 °C, the selec-

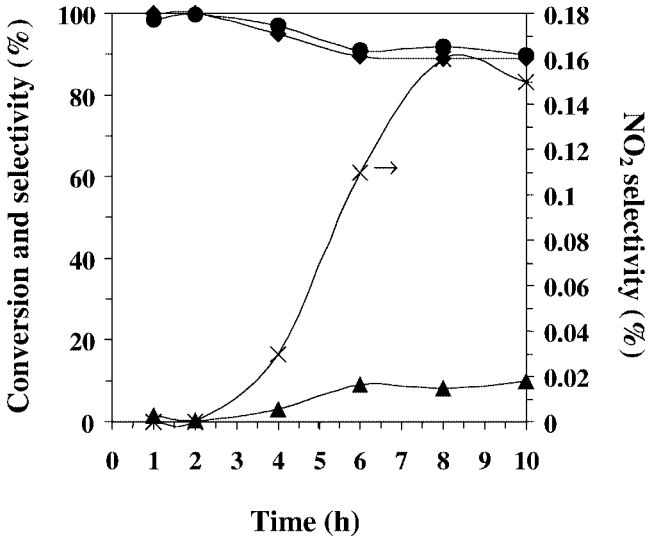

Figure 6. The activity of γ-Mo_2N in NO decomposition as related to the time of NO treatment at 450 °C: (•) NO conversion, (♦) N_2 selectivity, (▲) N_2O selectivity and (×) NO_2 selectivity.

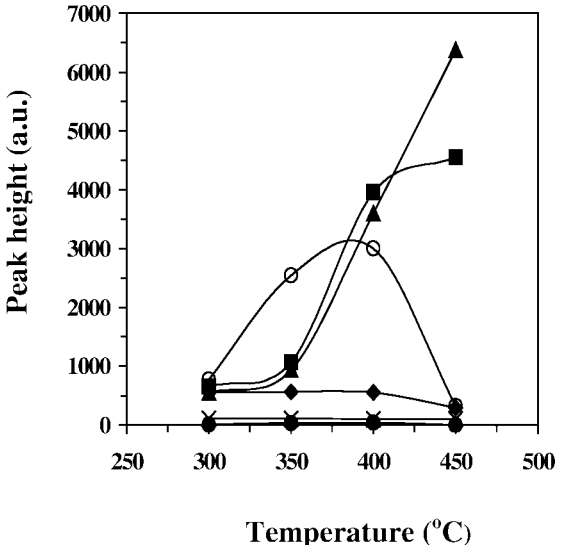

Figure 7. Product distribution in ^{15}NO pulsing over γ-Mo_2N: (▲) $^{15}N_2$, (■) $^{15}N^{14}N$, (○) $^{14}N_2$, (♦) $^{15}N^{14}NO$, (×) $^{15}N_2O$, and (•) $^{14}N_2O$.

tivities of N_2 over the two samples were roughly the same. At 450 °C, both materials showed a N_2 selectivity of ca. 98%. Besides N_2, N_2O was also a major product; its selectivity profile appeared as a mirror image of that of N_2. During the decomposition of NO, a trace amount of NO_2 was detected; the NO_2 signals decreased in intensity with temperature rise and disappeared at 350 and 450 °C over H_2-treated and passivated γ-Mo_2N, respectively.

When NO was pulsed over γ-Mo_2N, it decomposed into nitrogen and oxygen adspecies; while N_2, N_2O, and NO_2 desorbed into the gas phase, oxygen adatoms diffused into the pore and/or lattice of γ-Mo_2N until the material was saturated with oxygen. In order to examine the NO decomposition activity of the oxygen-saturated material, we treated a γ-Mo_2N sample in a flow of NO (15 ml min^{-1}) at 450 °C for 10 h and measured the decomposition activities at hourly intervals by means of NO-pulsing at the same temperature. The results are presented in figure 6. We observed that the NO conversion and N_2 selectivity were ca. 99% during the first 2 h and then decreased and reached ca. 95% at the 4th hour. After the 6th hour, NO conversion and N_2 selectivity stayed at ca. 89%.

3.2.2. Pulse reaction of ^{15}NO over passivated γ-Mo_2N

Figure 7 shows the results of ^{15}NO pulsing over passivated γ-Mo_2N at various temperatures. The detected species were $^{14}N^{15}NO$, $^{15}N_2O$, $^{14}N_2O$, $^{14}N_2$, $^{15}N^{14}N$, and $^{15}N_2$. No $^{15}NO_2$ and $^{14}NO_2$ were observed. From figure 7, one can see that the intensities of $^{15}N_2O$ and $^{14}N_2O$ were very low. The amount of $^{15}N^{14}NO$ formed was larger than that of $^{15}N_2O$ or $^{14}N_2O$. The amount of $^{14}N_2$ detected reached a maximum at ca. 400 °C and decreased to a low level at 450 °C. Between 350 and 450 °C, the intensities of $^{15}N^{14}N$ and $^{15}N_2$ increased with temperature rise. Table 1 shows the distributions of isotopic dinitrogen species at the 10th pulse of ^{15}NO. The contents of $^{15}N_2$, $^{15}N^{14}N$, and $^{14}N_2$ were

Table 1
Isotopic distributions of N_2 at the 10th pulse of ^{15}NO over passivated γ-Mo_2N.

Temperature (°C)	$^{15}N_2$ (%)	$^{15}N^{14}N$ (%)	$^{14}N_2$ (%)
300	31.3	36.7	32.0
350	36.4	41.6	22.0
400	44.4	48.8	6.8
450	56.8	40.0	3.2

31.3, 36.7, and 32.0%, respectively, at 300 °C; the contents of $^{15}N_2$ and $^{15}N^{14}N$ increased to 56.8 and 40.0%, respectively, whereas that of $^{14}N_2$ decreased to 3.2% at 450 °C. At 400 °C, a maximal distribution of $^{15}N^{14}N$ was observed. The results suggest that (i) NO adsorption was mainly dissociative above 450 °C and (ii) the infiltration of oxygen adatoms (generated in NO adsorption) into the nitrogen vacancies and/or lattice of γ-Mo_2N would result in the formation of a $Mo_2O_xN_y$ species.

3.3. Catalyst characterisation

3.3.1. XRD studies

Figure 8 shows the XRD patterns of passivated γ-Mo_2N before and after NO-pulsing (ca. 200 pulses of NO at 450 °C). The XRD patterns of the γ-Mo_2N samples after treatments at 450 °C in H_2 for 2 h, in NO for 10 h, and in H_2 for 1 h (after 10 h of NO treament) are also included. The diffraction pattern (figure 8(a)) of the fresh passivated γ-Mo_2N catalyst indicated that the γ-Mo_2N solid prepared by the TPN method was single-phase and cubic in structure. The intensity ratio of (200) and (111) reflections, $I(200)/I(111)$, has been used as a texture indication of γ-Mo_2N crystallites [3,10]. For the fresh, passivated γ-Mo_2N solid, the $I(200)/I(111)$ ratio was 1.24, much higher than that (0.5, JCPDS file data) of the randomly distributed uniform γ-Mo_2N crystallites, suggesting that the

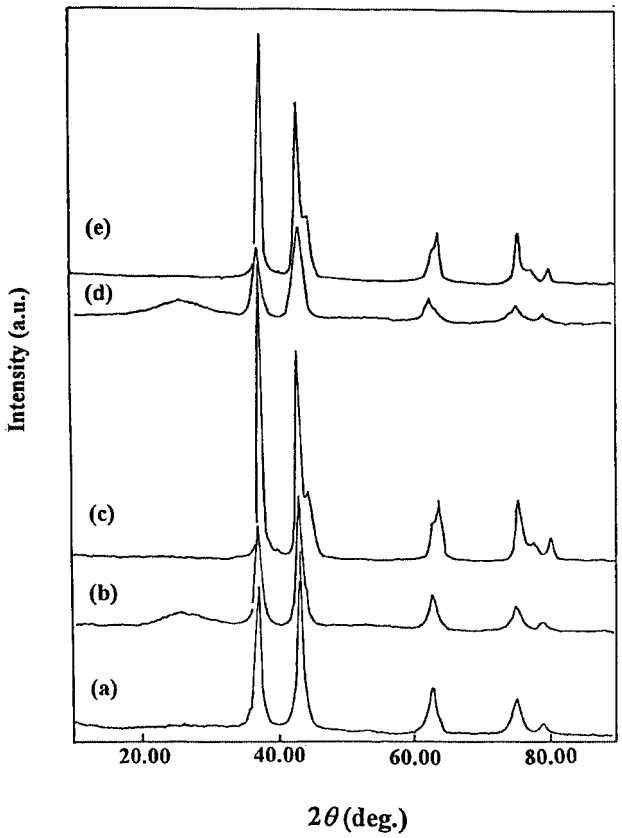

Figure 8. XRD patterns of passivated γ-Mo_2N: (a) fresh, (b) after NO pulsing, (c) after H_2 reduction, (d) after 10 h of NO treatment, and (e) after the NO-treated (10 h) sample was H_2 reduced.

alignment of crystallites is in the ⟨100⟩ direction. This type of texturing, which is a characteristic of high-surface-area γ-Mo_2N [13], was probably a consequence of the pseudomorphic nitridation of the MoO_3 particles into γ-Mo_2N. According to Choi et al. [13], the passivated γ-Mo_2N sample contained micro-sized and plate- or rod-like aggregates of much smaller nano-sized particles. After NO uptake and decomposition, a new amorphous-like phase with very weak signal centred at $2\theta = 25.9°$ was observed (figure 8(b)). This could be due to surface $Mo_2O_xN_y$ formed in NO dissociative adsorption on γ-Mo_2N. After H_2 treatment at 450 °C for 2 h, the crystal structure of γ-Mo_2N transformed from cubic to tetragonal (figure 8(c)). From figure 4, one can see that a tetragonal γ-Mo_2N was also active for NO decomposition. After the γ-Mo_2N material was treated in a flow of NO for 10 h, the XRD pattern recorded (figure 8(d)) was rather similar to that of figure 8(b), implying that a $Mo_2O_xN_y$ phase was formed in the oxygen-saturated γ-Mo_2N sample. After reducing of the oxygen-saturated γ-Mo_2N sample in H_2 at 450 °C for 1 h, the γ-Mo_2N phase was restored and there was not a trace of the $Mo_2O_xN_y$ phase (figure 8(e)).

3.3.2. TPR and TPD studies

Figure 9 illustrates the TPR profiles of passivated and O_2-treated γ-Mo_2N samples. For passivated γ-Mo_2N, there are two sharp bands at 340 and 850 °C and one broad band centered at 510 °C. The band at 340 °C might be due to the adsorption and diffusion of H_2 into the pores of γ-Mo_2N. The broad band at 510 °C could be assigned to the reduction of surface $Mo_2O_xN_y$. At 850 °C, γ-Mo_2N might react with H_2 to release N_2 and NH_3, yielding the second sharp band. Such a phenomenon has been reported by Wei et al. [14]. For O_2-treated γ-Mo_2N, there were a shoulder at 540 °C and a big band at 790 °C; the former was due to the reduction of oxygen adspecies, whereas the latter was due to the reduction of the partially oxidized γ-Mo_2N.

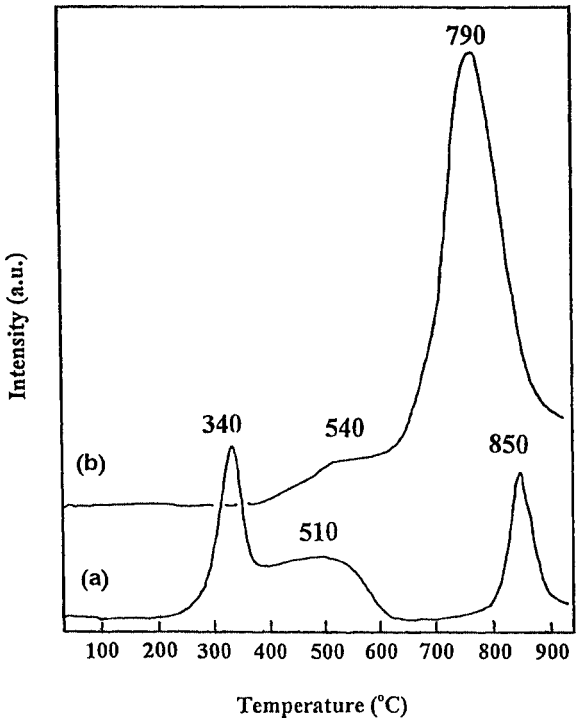

Figure 9. TPR profiles obtained over (a) fresh and (b) O_2-treated passivated γ-Mo_2N.

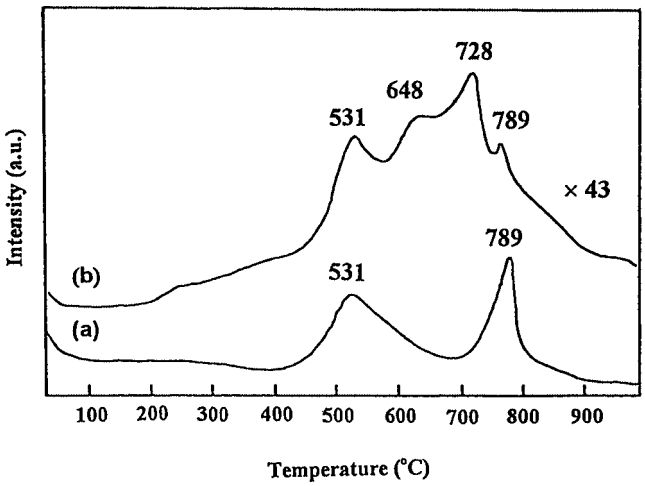

Figure 10. MS profiles of (a) N_2 and (b) N_2O obtained during NO-TPD study over passivated γ-Mo_2N.

Figure 10 shows the GC-MS profiles obtained during a NO-TPD study over the passivated γ-Mo_2N sample. Only

N_2 and N_2O were detected with the amount of the former larger than that of the latter. There were N_2 desorptions at 531 and 789 °C; the one at 531 °C could be due to the decomposition of adsorbed NO, whereas the other could be assigned to the desorption of lattice N atoms in γ-Mo_2N [14]. As for N_2O desorption, there were peaks observed at 531, 648, 728, and 789 °C. Such a complex profile suggests that there could be a number of ways for N_2O formation/desorption.

4. Discussion

The γ-Mo_2N particles reported here are porous (average pore diameter 43.1 Å) and cubic in structure. The material is nanometer (5.91 nm) in size and large in surface area (108 $m^2\,g^{-1}$). It has been reported that γ-Mo_2N shows a strong capability for O_2, H_2, NH_3, or NO adsorption [12] and exhibits good catalytic activities in ammonia synthesis and HDN reactions. In other words, γ-Mo_2N is capable of activating the N–H, N–O, and N–C bonds. Such a behavior would render γ-Mo_2N a good material for NO decomposition. Among the catalysts reported in the literature, the Cu-, Co-, Ce-, and Pt-exchanged zeolites [2] appear to perform well for direct NO decomposition. Previously, we reported the performance of perovskite-like oxide $La_{1.887}Th_{0.100}CuO_4$ [15] and 1 wt% Rh/CNTs (carbon nanotubes) [16] catalysts for this reaction; the temperatures required for 90% NO conversion were 650 and 500 °C, respectively. For the passivated and H_2-treated γ-Mo_2N materials reported in this Letter, nearly 100% NO conversion and 98% N_2 selectivity were achieved at 450 °C. When the passivated γ-Mo_2N material was saturated with oxygen, NO conversion and N_2 selectivity remained at ca. 89 and 91% (figure 6), respectively, indicating that the oxidized γ-Mo_2N material is catalytically active for NO decomposition.

The NO and O_2 storage capacities of the catalysts used in NO abatement and in three-way catalysts (TWCs) for automobile exhaust purification have received much attention [17]. Based on the fact that the XRD pattern of a NO-treated γ-Mo_2N sample (figure 8(d)) is rather similar to that obtained in NO adsorption (figure 8(b)), we deduce that after prolonged NO exposure, γ-Mo_2N was converted to $Mo_2O_xN_y$ rather than completely oxidized to MoO_3. Furthermore, the oxygen in $Mo_2O_xN_y$ could be removed via H_2 reduction. The recovery of the γ-Mo_2N phase after H_2 reduction at 450 °C (figure 8(e)) confirms that the material can be reduced and oxidized repeatedly in such cycles. The amount of oxygen that can be removed from $Mo_2O_xN_y$ amounted to ca. 93% of the total oxygen capacity, indicating that the catalyst exhibited a good OSC (oxygen storage capacity) behavior. Generally speaking, the larger the OSC value of a three-way catalyst is, the higher would be the NO conversion. Recently, CeO_2- and/or ZrO_2-supported metal catalysts have been intensively studied for this aspect. Working on catalysts with different contents of Pd, Ce, and Zr, Jen et al. [18] found that the 2 wt% Pd/CeO_2–ZrO_2 (CeO_2/ZrO_2 molar ratio = 7/3) catalyst was the most effective in storing oxygen, showing OSC value of 890, 970, and 1030 μmol g^{-1}, respectively, at 350, 520, and 700 °C. Compared to these values, the OSC value of γ-Mo_2N is even bigger. It should be pointed out that during the measurements for O_2 uptake over passivated γ-Mo_2N, we did not detect any N_2 among the effluent gases. The absence of N_2 suggests that oxygen could stay on the surface or diffuse into the pores and/or the lattice of γ-Mo_2N without displacing any N atoms. We deduce that after the uptake of O_2, there should be a $Mo_2O_xN_y$ species. The detection of a weak-intensity amorphous-like phase in XRD investigation (figure 8(b)) is a supporting evidence for this viewpoint. When NO was flowing through the catalyst continuously for 10 h, the nitrogen balance was estimated to be 100 ± 1%. Based on this fact and there was no N_2 detected in the effluent gases during O_2-pulsing, we suggest that the value of y in $Mo_2O_xN_y$ should be unity. The values of x estimated based on the amounts of O_2 uptakes at 300, 350, and 450°C were 0.08, 0.26, and 0.65, respectively. In TWCs, alkali or alkaline earth oxides are used to store NO via nitrate formation. For example, the NO uptake of a Pt−Rh−Ba−La−O catalyst supported on a washcoat was 20 mg $g_{cat.}^{-1}$ at 350 °C [19]and that of BaO was 15 mg $g_{cat.}^{-1}$ at temperature below 500 °C under lean-burn conditions [20]. For the γ-Mo_2N material, the NO uptakes were 3.6 mg $g_{cat.}^{-1}$ (119 μmol $g_{cat.}^{-1}$) and 5.5 mg $g_{cat.}^{-1}$ (182.7 μmol $g_{cat.}^{-1}$), respectively, at 50 and 400 °C. Obviously, the mechanism for NO uptake over the γ-Mo_2N catalyst is different from that over the BaO-containing catalysts. Over γ-Mo_2N, NO adsorbed dissociatively with N_2 desorption at ca. 531 °C (figure 10(a)). In other words, the dissociative adsorption of NO over γ-Mo_2N is an activated action.

When O_2 or NO was pulsed over the γ-Mo_2N catalyst, a $Mo_2O_xN_y$ phase was generated via the incorporation of oxygen in the γ-Mo_2N lattice. As the amount of O_2 or NO introduced into the reaction system increased, the content of oxygen in the sample increased and reached its limit, such as $x = 0.65$ at 450 °C with the γ-Mo_2N material being converted into $Mo_2O_{0.65}N$. During the 10 h of NO treatment (figure 6), NO conversion recorded in a pulse of NO at 450 °C reduced from an initial value of ca. 99–89% at the 6th hour. It is likely that in the early hours NO reacts with γ-Mo_2N chemically, whereas after the 6th hour, NO decomposition was entirely catalytic over the oxygen-saturated material, such as $Mo_2O_{0.65}N$ at 450 °C. The high level of NO conversion (ca. 89% at 450 °C) indicates that the $Mo_2O_xN_y$ phase is active catalytically for NO removal.

Due to the fact that γ-Mo_2N was prepared by reacting of MoO_3 with NH_3, it is possible that there were NH_x adspecies accumulated on the material. Haddix et al. [21] suggested that ammonia could be adsorbed on nitrogen vacancies and partly converted into NH_2 and/or NH adspecies. Thompson and co-workers [22] reported that a considerable amount of NH_3 desorbed from a passivated Mo_2N sample in the temperature region of 200−300 °C. The pretreatment of the passivated Mo_2N catalyst in He at 450 °C for 1 h was to ensure the complete removal of surface NH_x adspecies. Ac-

cording to the results of the ^{15}NO-pulsing experiments, we propose that below 450 °C, NO adsorbed on γ-Mo_2N in the form of a complex (**A**):

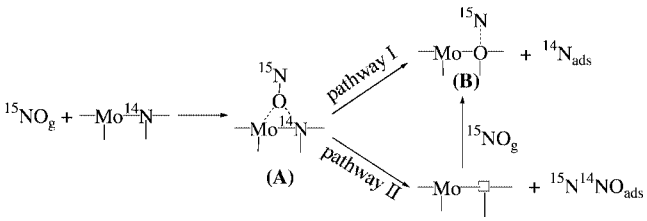

(2)

In pathway I, the oxygen atom, being more electronegative than the nitrogen atom, attacks a nearby Mo atom and drives a lattice N atom to the surface, resulting in the formation of intermediate (**B**). The ^{15}N and ^{14}N adspecies could couple at roughly the same chance to form $^{15}N_2$, $^{15}N^{14}N$, and $^{14}N_2$. The similarity in $^{15}N_2$, $^{15}N^{14}N$, and $^{14}N_2$ distributions in ^{15}NO pulsing at 300 °C (table 1) substantiates the above deduction. In pathway II, the release of $^{15}N^{14}NO$ in the interaction of ^{15}NO with Mo−^{14}N would create a nitrogen vacant site. The adsorption of a ^{15}NO molecule at this vacancy could also generate intermediate (**B**). As reflected in the small amount of $^{15}N^{14}NO$ detected, pathway I was preponderant over pathway II in NO decomposition. We propose that at or above 450 °C, ^{15}NO dissociation proceeds according to

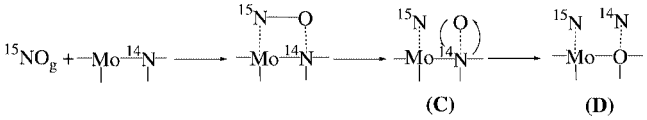

(3)

Due to the diffusion of oxygen, a certain amount of (**C**) is converted to (**D**) before the γ-Mo_2N sample was saturated with oxygen.

According to the above results, we deduce that (i) NO adsorption above 450 °C was mainly dissociative and (ii) there was formation of $Mo_2O_xN_y$. The decreases in N_2O and NO_2 selectivities with temperature rise and the absence of N_2O and NO_2 at 450 °C (figure 5 (b) and (c)) are supporting evidence for (i). The appearance of a weak-intensity, amorphous-like phase (figure 8(b)) after NO decomposition is a proof for (ii). We have illustrated that the $Mo_2O_xN_y$ material is catalytically active for the direct decomposition of NO.

References

[1] K. Tamaru and G.A. Mills, Catal. Today 22 (1994) 349.
[2] V.I. Parvulescu, P. Grange and B. Delmon, Catal. Today 46 (1998) 233.
[3] S.W. Yang, C. Li, J. Xu and Q. Xin, J. Phys. Chem. B 102(1998) 6986.
[4] G.S. Ranhotra, A.T. Bell and J.A. Reimer, J. Catal. 108 (1987) 40.
[5] M. Boudart, S.T. Oyama and L. Leclercq, in: *Proc. 7th Int. Congr. on Catalysis*, Tokyo (Elsevier, Amsterdam, 1981) p. 578.
[6] E.J. Markel and J.W. VanZee, J. Catal. 126 (1990) 643.
[7] C.W. Colling and L.T. Thompson, J. Catal. 146 (1994) 193.
[8] C.W. Kim, D.K. Lee and S.K. Ihm, Catal. Lett. 43 (1997) 91.
[9] M. Nagai, Y. Goto, A. Miyata, M. Kiyoshi, K. Hada, K. Oshikawa and S. Omi, J. Catal. 182 (1999) 292.
[10] M. Nagai, Y. Goto, A. Irisawa and S. Omi, J. Catal. 191 (2000) 128.
[11] J.G. Choi, J.R. Brenner, C.W. Colling, B.G. Demczyk, J.L. Dunning and L.T. Thompson, Catal. Today 15 (1992) 201.
[12] X.S. Li, J. Xu and L.W. Lin, *Advanced Reactions and Materials in Catalysis* (Henan Science and Technology Publisher, 1996).
[13] J.G. Choi, R.L. Curl and L.T. Thompson, J. Catal. 146 (1994) 218.
[14] Z.B. Wei, Q. Xin, P. Grange and B. Delmon, J. Catal. 168 (1997) 176.
[15] L.Z. Gao and C.T. Au, Catal. Lett. 65 (2000) 91.
[16] J.Z. Luo, L.Z. Gao, Y.L. Leung and C.T. Au, Catal. Lett. 66 (2000) 91.
[17] R.J. Farrautox and R.M. Heck, Catal. Today 51 (1999) 351.
[18] H.W. Jen, G.W. Graham, W. Chun, R.W. McCabe, J.P. Cuif, S.E. Deutsch and O. Touret, Catal. Today 50 (1999) 309.
[19] H. Mahzoul, J.F. Brilhac and P. Gilot, Appl. Catal. B 20 (1999) 47.
[20] S. Hodjati, P. Bernhardt, C. Petit, V. Pitchon and A. Kiennemann, Appl. Catal. B 19 (1998) 209.
[21] G.W. Haddix, D.H. Jones, J.A. Reimer and A.T. Bell, J. Catal. 112 (1988) 556.
[22] C.W. Colling, J.G. Choi and L.T. Thompson, J. Catal. 160 (1996) 35.